Available online at www.sciencedirect.com
ScienceDirect
Cryogenics 47 (2007) 457–467
Cryogenics
www.elsevier.com/locate/cryogenics

# Study on static and dynamic characteristics of moving magnet linear compressors

N. Chen [a], Y.J. Tang [b], Y.N. Wu [b], X. Chen [b], L. Xu [a,*]

[a] Institute of Refrigeration and Cryogenics, Shanghai Jiaotong University, 1954 Huashan Road, Shanghai 200030, PR China
[b] Shanghai Institute of Technical Physics, Chinese Academy of Sciences, 500 Yu Tian Road, Shanghai 200083, PR China

Received 5 June 2006; received in revised form 4 March 2007; accepted 16 March 2007

**Abstract**

With the development of high-strength NdFeB magnetic material, moving magnet linear compressors have been gradually introduced in the fields of refrigeration and cryogenic engineering, especially in Stirling and pulse tube cryocoolers. This paper presents simulation and experimental investigations on the static and dynamic characteristics of a moving magnet linear motor and a moving magnet linear compressor. Both equivalent magnetic circuits and finite element approaches have been used to model the moving magnet linear motor. Subsequently, the force and equilibrium characteristics of the linear motor have been predicted and verified by detailed static experimental analyses. In combination with a harmonic analysis, experimental investigations were conducted on a prototype of a moving magnet linear compressor. A voltage–stroke relationship, the effect of charging pressure on the performance and dynamic frequency response characteristics are investigated. Finally, the method to identify optimal points of the linear compressor has been described, which is indispensable to the design and operation of moving magnet linear compressors.
© 2007 Published by Elsevier Ltd.

*Keywords:* Moving magnet linear compressor; Force; Frequency; Performance

## 1. Introduction

Linear free piston compressors are employed in a wide range of reciprocating electro-mechanical actuation systems, from domestic refrigerators, Stirling cycle and pulse tube cryocoolers, to fuel pumps and artificial heart devices. They are usually required to be efficient and reliable, typically offering 20,000 h of maintenance free operation. Moreover, they must also meet demands for functionality and cost, whilst fulfilling minimum volume and loss criteria [1]. Linear motors which are the heart of the linear compressor can be of three different types, i.e. moving coil, moving magnet and moving iron. The moving iron type is scarcely used due to the heavy moving parts and small force. The moving magnet and moving coil motors have their own advantages and disadvantages. Flying leads in the moving coil motor is a potential source of unreliability and limits the achievable stroke. On the contrast, due to the windings bonded directly to a yoke in the moving magnet motor, the good thermal dissipation characteristics, low material outgassing rate and high reliability can be obtained. Moreover, the required volume of the permanent magnet (PM) in the moving magnet configuration is much smaller than that needed by the moving coil configuration of same power output and efficiency. All above characteristics make the moving magnet configuration more suitable to be used in the linear compressor [2]. Recently, the increasing number of moving magnet linear compressors has been used in some important space missions [3,4].

Redlich et al. [1] introduced a type of linear motor, whose shuttle consisted of a ferromagnetic core and a homopolar, radially magnetized, bonded PM ring, a stator comprised a pair of coils, wound in series opposition and an outer ferromagnetic sleeve (see Fig. 1). This topology has been widely used in gas compressors. From the

* Corresponding author. Tel./fax: +81 21 6293 3251.
*E-mail addresses:* xulie@sjtu.edu.cn, chennan@sjtu.edu.cn (L. Xu).

0011-2275/$ - see front matter © 2007 Published by Elsevier Ltd.
doi:10.1016/j.cryogenics.2007.03.011

IPR2024-00569
Sony EX1018 Page 1

**Nomenclature**

| | |
|---|---|
| $B$ | magnetic density, T |
| $D$ | damp, N s/m |
| $e$ | back voltage, V |
| $F$ | force, N |
| $H$ | magnetic potential, A/m |
| $i$ | current, A |
| $I$ | effective value of current, A |
| $j$ | imaginary part of complex |
| $K$ | stiffness, N/m |
| $l$ | length, mm |
| $L$ | inductance, H |
| $M$ | mass, kg |
| $N$ | number of windings |
| $p$ | power, W |
| $P$ | pressure, Pa |
| $r$ | radius, mm |
| $R$ | electrical resistance, Ω |
| $S$ | area, $m^2$ |
| $t$ | time, s |
| $T$ | period, s |
| $v$ | voltage, V |
| $V$ | volume, $m^3$ |
| $W$ | co-energy, J |
| $x$ | displacement from balance point, mm |

*Greek symbols*

| | |
|---|---|
| $\eta$ | efficiency, % |
| $\theta$ | phase angle, rad |
| $\mu$ | relative magnetic permeability |
| $\phi$ | magnetic flux, Wb |
| $\psi$ | flux linkage, Wb Turn |
| $\omega$ | angular frequency, rad/s |

*Superscripts*

| | |
|---|---|
| a | amplitude |
| c | coercive |
| Cu | copper |
| e | equivalent |
| g | gas |
| in | input |
| iron | yoke iron |
| m | mechanical |
| max | maximum |
| mean | mean value |
| mover | piston and actuator of motor |
| n | natural frequency |
| o | operation |
| p | permanent magnet (PM) |
| pl | left PM |
| pr | right PM |
| r | remnant magnet |
| s | spring |
| t | piston |
| V | virtual |
| w | wall |
| 0 | vacuum |

viewpoint of electro-mechanical energy conversion, the electrical energy in the exciting circuit is converted into mechanical energy by means of induced electromotive force (EMF) produced by the periodical variation of magnetic flux in an air gap. So the distribution and organization of the magnetic field in the air gap have great effects on the motor performance. Until now, the equivalent magnetic circuit analysis and finite element analysis (FEA) are two of the most effective methods in the magnetic field analysis.

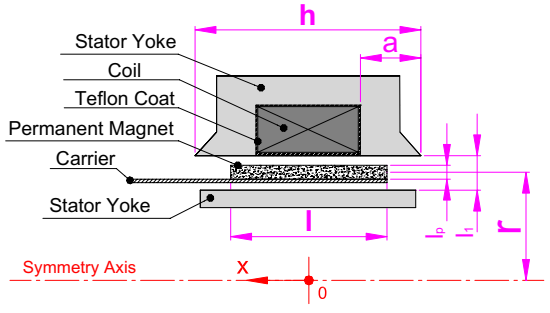



Fig. 1. Definitions of the geometrical dimensions of the moving magnet linear motor.

For the equivalent magnetic circuit analysis, Longthworth [5] gave the simplified expression of force and back EMF, and the engineering design and construction method of a dual PM linear motor in a Stirling cryocooler was introduced. Byckling and Perkio [6] developed the equations of motion, force and the equivalent circuit of a moving magnet transducer for a loudspeaker. It was pointed out that the moving magnet transducer had low pass and high-frequency cut-off characteristics. Yang et al. [7] gave the analytical solution of the electromagnetic force of a linear oscillating motor and simulated the field, force and dynamics respectively. Poornima and Hsu [8] gave the expressions of force and the electrical power converted to produce motion in a moving magnet loudspeaker system. Ebihara and Watada [9] discussed the static thrust and frequency characteristics of a linear oscillatory actuator used in an artificial heart. The maximum static thrust was measured at approximately 72 N and the starting thrust at approximately 20 N. Clark et al. [10,11] presented an optimum design method of the linear motor based on the FEA. The Coil inductance and peak force/amp of their prototype actuator were 1.65 mH and 8.0 N/A, respectively. These investigations show that the FEA is an effective method

IPR2024-00569
Sony EX1018 Page 2

to get the distribution parameters of the magnetic field in the linear motor. Although the variation of force along the stroke was actually observed in the experiments [9,10,12], the electromagnetic force along the whole stroke was still regarded as a constant in majority of above-mentioned papers. For the practical application of the moving magnet linear compressors, this characteristic is very important owing to the increasing gas stiffness in the process of compression.

Another two important aspects of the moving magnet linear compressor are the thermodynamic process of working gas and the dynamic process of the piston, both of which are similar to the moving coil linear compressor. Many previous papers [13–17] reported the dynamic characteristics of the moving coil compressors, in which the effect of the compressed gas on the piston had been expressed by an equivalent damping coefficient and a gas spring stiffness. The simulating results of the actuator are in good agreement with experimental data.

Although Sunpower Inc. produced a series of high performance Stirling and pulse tube cryocoolers based on the moving magnet linear compressors, almost all published papers [18–20] introduced the performance as a whole rather than the detail analysis of the parameters. Philips Laboratories [21] provided a simplified design method of the moving magnet linear compressor for the Stirling cooler. However, the variation of the electromagnetic force and inductance of the coil were ignored.

In this paper, the force of a linear motor, as the function of geometrical parameters, input current and magnetic potential of the PM is firstly deduced from the magnetic circuit analysis. Then, the FEA was used to obtain the distribution of the magnetic field in the linear motor. Based on the experimental measurements, the static performance of the linear motor, including force and equilibrium characteristics have been studied. Furthermore, in order to investigate the performance of a linear compressor comprehensively, a mathematical model has been developed, in which the static force model, thermodynamic and electrical circuit model have been involved. Based on harmonic assumptions, the two dimensional control equations of linear compressors have been solved and consequently the dynamic characteristics of the linear compressor have been revealed by a series of equations. As the result, the corresponding equivalent electrical circuit of a linear compressor is presented, by which the compressor can be regarded as a simple input and output module. Finally, a prototype of the moving magnet linear compressor was constructed and tested. Theoretical solutions have been verified by the experimental data and many useful results are presented.

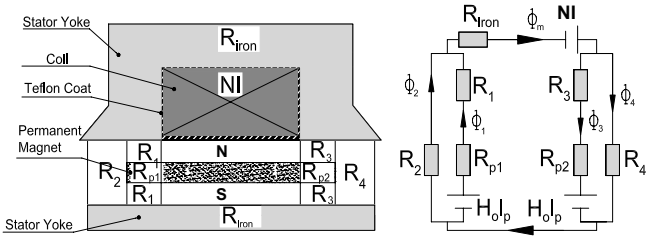



Fig. 2. Magnetic equivalent circuit of the moving magnet linear motor.

## 2. Moving magnet linear motors

### 2.1. Magnetic circuit model of linear motors

The electromagnetic force of linear motor depends on the interaction field between the exciting coil and the PM. Referring to the theory of electromagnetic analogy, the magnetic circuit of the moving magnet linear motor can be simplified as shown in Fig. 2, where the linear $B$–$H$ characteristics of the PM and the lumped approximation of the distributed flux are adopted [6]. The quantity $\phi_1$ is the flux in the air gap which goes through the permanent magnet and that of $\phi_2$ is the flux that bypass it. The quantity $H_0$ is the coercive force of the PM, and $N$ and $I$ are the number of turns and current of the driving coil. Due to linear assumptions of the magnetic circuit, the magnetic co-energy of this system in Eq. (1) can be divided into three parts which correspond to three sources of the magnetic potential in Fig. 2 respectively

$$\begin{aligned} W(i_{\mathrm{Vpl}}, i_{\mathrm{Vpr}}, i, x) = & \int_{\mathrm{Path1}} \mathrm{d}W(i, i_{\mathrm{Vpl}} = i_{\mathrm{Vpr}} = 0, x) \\ & + \int_{\mathrm{Path2}} \mathrm{d}W(i_{\mathrm{Vpr}}, i_{\mathrm{Vpl}} = 0, i = I, x) \\ & + \int_{\mathrm{Path3}} \mathrm{d}W(i_{\mathrm{Vpl}}, i = I, , i_{\mathrm{Vpr}} = I_{\mathrm{Vpr}}, x), \end{aligned} \tag{1}$$

where Path1, Path2 and Path3 indicate three different integrating paths to get the magnetic co-energy ($W(I_{\mathrm{Vpl}}, I_{\mathrm{Vpr}}, I)$). The variables of $i_{\mathrm{Vpl}}$ and $i_{\mathrm{Vpr}}$ are respectively defined as the virtual currents, which can bring up the same magnetic potential of driving coil as that of the PM [22]. The quantity of $I_{\mathrm{Vpr}}$ and $I_{\mathrm{Vpl}}$ are their corresponding values of NdFeB. Based on Ohm's and Kirchhoff's law of the magnetic circuit, the energy stored in the system is $x$

$$\begin{aligned} \int_{\mathrm{Path1}} \mathrm{d}W &= \int_0^I N\phi(i, i_{\mathrm{Vpl}} = i_{\mathrm{Vpr}} = 0, x)\,\mathrm{d}i \\ &= \frac{1}{2}(NI)^2 \frac{(R_1 + R_2 + R_{P1})(R_3 + R_4 + R_{P2})}{R_2(R_1 + R_{P1})(R_3 + R_4 + R_{P2}) + R_4(R_3 + R_{P2})(R_1 + R_2 + R_{P1}) + R_{\mathrm{iron}}(R_1 + R_2 + R_{P1})(R_3 + R_4 + R_{P2})}, \end{aligned} \tag{2}$$

IPR2024-00569
Sony EX1018 Page 3

where $R_1$, $R_2$, $R_3$ and $R_4$ are the reluctances of the air gap corresponding to the magnetic flux $\phi_1$, $\phi_2$, $\phi_3$ and $\phi_4$, respectively; $R_{p1}$ and $R_{p2}$ are the reluctances of the PMs, respectively; $R_{\text{iron}}$ is the reluctance of the iron core.

In the same way, $W_{\text{Path2}}$ and $W_{\text{Path3}}$ can be obtained by integration of their own paths, as follows:

$$W_{\text{Path2}} = \frac{(p_1 + R_2 + R_{\text{iron}})(H_o l_p)^2/2 - R_2 NIH_o l_p}{R_2(p_1 + R_{\text{iron}}) + (R_1 + R_{P1})(p_1 + R_2 + R_{\text{iron}})}, \quad (3)$$

and

$$W_{\text{Path3}} = \frac{q_1}{M} R_2 NIH_o l_p + \frac{(H_o l_p)^2}{M}\left[\frac{R_2}{2}(q_1 - q_2) + q_1 R_m - q_2 R_4\right], \quad (4)$$

where the intermediate variables are

$$p_1 = R_4(R_3 + R_{p2})/(R_3 + R_4 + R_{p2}),$$
$$q_1 = R_2 R_4 + R_4(R_1 + R_{p1}),$$
$$q_2 = R_2 R_{\text{iron}} + (R_2 + R_{\text{iron}})(R_1 + R_{p1}),$$

and

$$M = [R_2 R_4 + R_2(R_3 + R_{p2})][(R_2 + R_{\text{iron}})(R_1 + R_{p1}) + R_2 R_{\text{iron}}] + R_2(R_3 + R_{p2})[R_2 R_4 + R_4(R_1 + R_{p1})].$$

Then, the electromagnetic force equals the partially derivative of the $W$ in Eq. (1) with respect to the displacement ($x$), that is

$$f = \left.\frac{\partial W}{\partial x}\right|_{i_{\text{Vpl}}, i_{\text{Vpr}}, i}. \quad (5)$$

Substituting the result of Eq. (1) into Eq. (5), the electromagnetic force is

$$f = -\frac{2\pi r\mu_0}{l_1} H_o l_p NI - \frac{2\pi r\mu_0}{l_1}\frac{x}{a}(H_o l_p)^2 + \frac{2\pi r\mu_0}{l_1}\frac{2x}{h - l}(NI)^2, \quad (6)$$

which indicates that the driving current, geometrical parameters and characteristics of the PM have close relationship with the force. The first term actually represents interacting force between the PM and the coil. The last two terms are the functions of the displacement and become zero in the central position. By the dimensional analysis, it was found that the absolute value of the first part is larger than that of the last two parts.

In practice, the operating point of the PM actually varies along the magnetization line. $H_o$ in Eq. (6) is the magnetic potential of the operating point instead of the coercive force ($H_c$). As for the NdFeB, the magnetization line in the second quadrant can be approximately expressed as a linear function, $B = -HB_r/H_c + B_r$. The operation point along the magnetization line is determined by the flux across the PM. Assuming the summary of the magnetic potential provided by the PM is $H_o l_p$, according to the continuity of the magnetic potential ($NI = H_o l_p + \phi R$), and substituting this expression into the first term of Eq. (6), one can get $f = -\frac{2\pi r\mu_0}{l_1} H_o l_p (H_o l_p + \phi R)$. When $NI = -H_o l_p = R\phi/2$, the maximum force can be obtained. However it should be pointed out that it is impossible to raise $NI$ infinitely by increasing the input current in reference to the limit varying range of $H_o(0, H_c)$. So, the maximum permitted current ($i_{\max}$) is confined by $H_c l_p = N i_{\max}$. In other words, the maximum permitted peak current is $i_{\max} = H_c l_p/N$ so that the maximum force is $f_{\max} = 2\pi r\mu_0 H_o H_c l_p^2/l_1$. This expression is the theoretical value of the force. In order to make full use of the PM, the operation point of the PM should vary closely to the point with the maximum magnetism energy produce. As to the NdFeB, the coercive force of this point is about $0.5H_c$. Therefore, in the design of linear motors, both magnetic circuit organization and property of PM should be considered comprehensively.

According to the Faraday's law of the electromagnetic induction, the induced back EMF applied on the exciting coil can be expressed as

$$e = \left(\frac{\partial \psi}{\partial i}\right)\frac{\mathrm{d}i}{\mathrm{d}t} + \left(\frac{\partial \psi}{\partial x}\right)\frac{\mathrm{d}x}{\mathrm{d}t}, \quad (7)$$

where the $\Psi$ is the coil flux linkage.

Referring to Fig. 2, the induced back EMF on the exciting coil can be obtained by the magnetic circuit analysis. That is

$$e = N^2 \frac{\pi r\mu_0 a}{l_1}\cdot\frac{\mathrm{d}i}{\mathrm{d}t} - NH_0 l_p \frac{2\pi r\mu_0}{l_1}\cdot\frac{\mathrm{d}x}{\mathrm{d}t}. \quad (8)$$

By means of dimensional analysis, it is found that the quantity of the inductive voltage (the first term of Eq. (8)) is far less than that of the speed voltage (the second term of Eq. (8)). So, the majority of the electrical energy is actually converted into the mechanical energy by the virtue of the speed voltage.

### 2.2. Static performance of linear motors

The static force–displacement characteristic, i.e. the relationship between the electromagnetic force exerted on the moving PM and its axial displacement under different direct currents applied on the exciting coil, is one of key indexes to the linear motor. The magnetic field distribution and the magnetic force without exciting current also have great influence on linear motor applications.

The parameters of the geometrical dimension, electrical configuration and material property are given in Table 1. The diameter of the investigated linear motor stator (see Fig. 3) is 120 mm, the length is 65 mm and the mass is 2.21 kg. In order to reduce the Joule heat ($I^2R$), the large-diameter copper wire was wound tightly on the yoke. The total electric resistance of the coil is 0.41 Ω. The magnetic circuit is formed by ferrite, which can effectively reduce the core loss. The diameter of the corresponding aluminum armature, attached by the lamellar NdFeB-35 PM, is 72 mm and its mass is 0.41 kg. The static characteristics of this motor were investigated on a modified C620H

IPR2024-00569
Sony EX1018 Page 4

Table 1
Parameters of the moving magnet linear compressor

| | | | |
|---|---|---|---|
| *Linear motor* | | | |
| Magnet material | | Coil and yoke | |
| Relative permeability | 1.0998 | Outer diameter (mm) | 94 |
| Coercivity (A/m) | $-8.9 \times 10^5$ | Inner diameter (mm) | 76 |
| Retentivity (Tesla) | 1.23 | Coil wire size (mm) | 1.5 |
| Thickness (mm) | 4 | Number of turns | 150 |
| Magnetization direction | Radial | | |
| Actuator | | Coil resistance (Ω) | 0.41 |
| Length (mm) | 45 | Max. current (A) | 15 |
| Diameter (mm) | 73 | Max. electrical input (W) | 250 |
| Mass (g) | 410 | Distance between internal and external yoke (mm) | 6 |
| *Integral linear compressor* | | | |
| Frequency (Hz) | 45–65 | Total stiffness of spring (N/m) | 2316 |
| Max. displacement (mm) | 10 | Total mass of spring (g) | 622 |
| Diameter of cylinder (mm) | 45 | Total mass of mover (g) | 560 |
| Volume of gas bank ($cm^3$) | 141 | Clearance seal (μm) | 10–20 |
| Working gas | Helium | | |



Fig. 3. Stator of the linear motor.

machine tool (see Fig. 4), on which the force and displacement could be conveniently regulated and kept coaxial. An ergometer (TK-10) and a slide calliper were used to measure the force and displacement respectively. In addition, magnetic field analysis software (Ansoft Maxwell) was used to get the optimum distribution of the magnetic field. By adopting different profiles of the yoke, even distribution of flux in the air gap had been obtained, at the same time the maximum value of flux was kept less than the magnetic saturation point of the ferrite.

Fig. 5 presents the FEA results of the magnetic filed distribution in the linear motor. It was found that the magnetic field in the air gap is the superposed fields of the PM and the exciting coil. From the density difference of flux at two ends of the moving PM (Fig. 5a), it is evident that the force directs upward and the subsequent motion is to offset this difference. The flux lines are not parallel with each other in the air gap, especially at the both ends of the PM. It means that there exist axial and radial components of the force. The axial component is the useful part and the radial component counteracts circumferentially. Due to the proper section configuration of the yoke, the eddy current is actually not obvious. The maximum flux density can be kept less than 2.0 T and the magnetic saturation can be avoided. However, there exists weak leakage of flux at the end of the yoke because of the limited dimensions.

According to the equipotential line of the magnetic potential (see Fig. 5b), it was found that the operating potential of the PM is actually far less than the coercive force of NdFeB-35. In the practical operation, the flux density across the PM rarely declines to zero. Based on Fig. 5b, the practical operating point of the PM can be approximately obtained.

In a moving coil linear motor, the magnetic force in the air gap depends on the existence of exciting current. On the contrast, the static force equilibrium of the PM in the moving magnet linear motor is more complex. Without exciting current, the magnetic force is still applied on the PM. In order to investigate this special phenomenon, both an experimental study and a FEA have been conducted.

In the experimental study, the magnetic force was measured when the stroke of the PM range from 0 mm to 9.0 mm. As shown in Fig. 6, when the PM is in the central

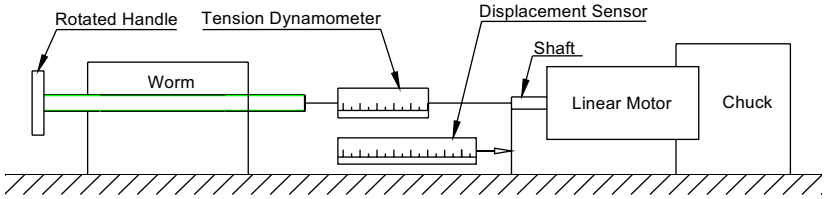



Fig. 4. Schematic of the static characteristic testing bench.

IPR2024-00569
Sony EX1018 Page 5

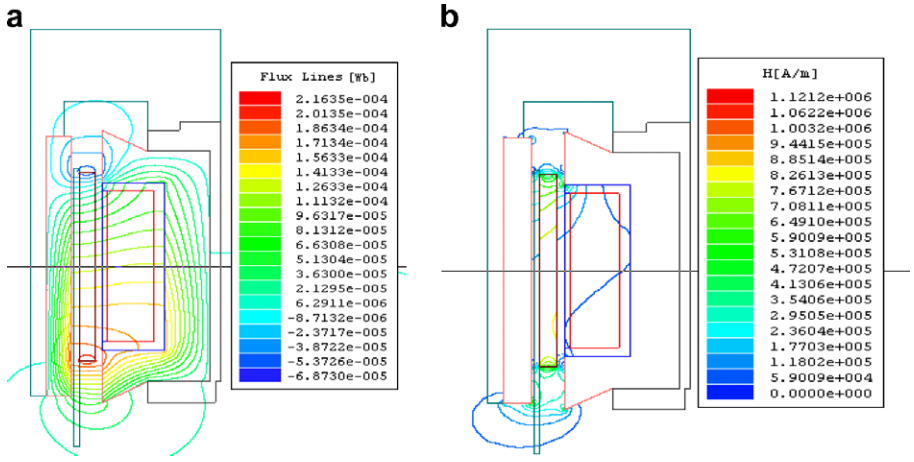



Fig. 5. The magnetic field distribution at the exciting current of 9 A. (a) Magnetic flux. (b) Magnetic potential.

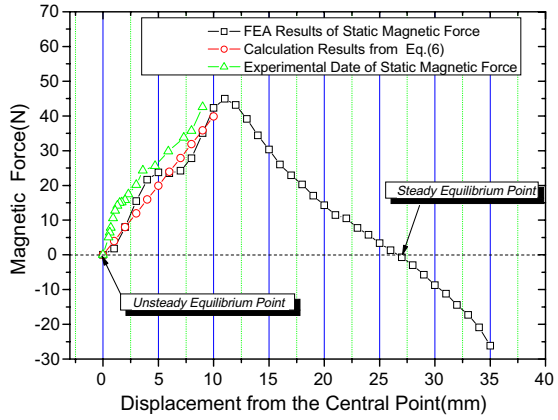



Fig. 6. Magnetic force without exciting current with displacement of the shuttle.

position, the composite magnetic force applied on the PM is equal to zero. However, it was observed that once the disturbance is applied, the magnetic force will increase rapidly with the increase of displacement. In the experiments, the increasing rate is about 4 N/mm. As a result, the equilibrium will be broken easily. Hence, this state can be regarded as the unsteady equilibrium.

This magnetic force characteristic without the exciting current should be considered in advance in the design of the linear motor. Once the PM leaves the central point due to the inevitable outside distribution, enough spring stiffness should be provided to avoid large offset displacement. Under this off-center condition, more input current should be provided to ensure the oscillation around the central point. It also means the enough input current should be provided to ensure that the first term in Eq. (6) is larger than the last two terms.

When the displacement increases to 11 mm continuously, the magnetic force correspondingly reaches the maximum value of 45 N according to the FEA results. Then, this force begins to reduce gradually and finally becomes zero when the displacement is about 26 mm. Similar to that of the central point, the composite force at this point is also equal to zero. However, the essential difference between these two points is that the magnetic force is negative (see Fig. 6) when the displacement is larger than 26 mm. It means that once the PM leaves this point, the magnetic force will draw it back. So the state of this point can be considered as a steady equilibrium. The position of this point in the experimental study was 24.4 mm, which is close to the result of the FEA.

The force characteristics of these two equilibrium points imply that, due to the inevitable disturbance, the piston of the linear compressor actually deflects its central point, which results in a reduction of the compressing stroke. Therefore, this factor should be considered in the design of mechanical springs to avoid the excess deflection. This force has close relation to the geometrical dimension of the yoke and PM. According to Eq. (6), if the dimension of the air gap and the diameter of the yoke are constant, the force should be the function of $2/(h-l)-1/a$. When $2a = h - l$, referencing to Fig. 1, this force will tend to zero. Hence, this force can be reduced significantly by increasing the length of the yoke.

Using three different methods, i.e. experimental measurement, theoretical calculation from Eq. (6) and FEA respectively, the relation between the axial displacement and the force at the exciting current of 11 A is illustrated in Fig. 7. It is shown that the electromagnetic force declines with the increase of the displacement. For example, the force declines about 23.8% with the displacement varying from 0 mm to 8 mm. It can also be found that both the FEA and linear magnetic circuit analysis are the effective approaches to study the force–displacement characteristics of the linear motor. Due to the existence of the flux leakage at the end of the stroke, which had not involved in the magnetic circuit model, there is about 20% discrepancy at full stroke.

It was found from Fig. 8 that the electromagnetic force at the central position increases when the exciting current increases from 6 A to 11 A. When the PM is at the central

IPR2024-00569
Sony EX1018 Page 6

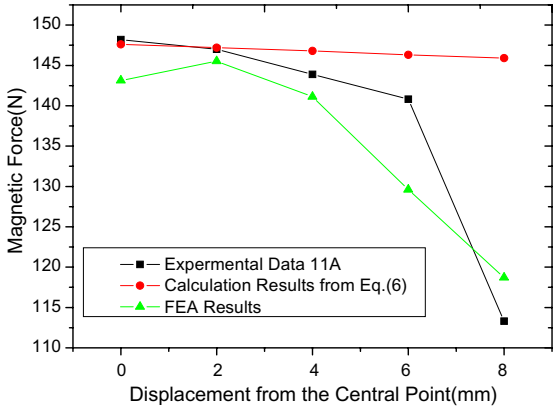



Fig. 7. Variation of the electromagnetic force with the displacement.

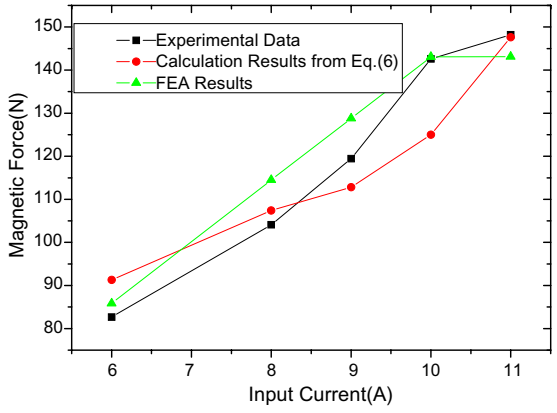



Fig. 8. Variation of the magnetic force with the input current.

position and the current increases from 6 A to 9 A and 9 A to 11 A, the corresponding increment rate of the force are 44.06% and 23.08% respectively. It can also be observed that the input current is approximated proportional to the force when the actuator is located at the central point. The comparison between the results from the FEA and Eq. (6) with the experimental data shows the validity of the theoretical analysis to predict the force characteristics of the linear motor.

## 3. Theoretical analysis of linear compressors

### 3.1. Mathematical model of linear compressors

The voltage equation for the driving circuit of a linear motor can be expressed as

$$v(t) = iR + e. \tag{9}$$

The mechanical force balance of the moving PM screwed on the piston results in the following equation

$$M\frac{\mathrm{d}^2x}{\mathrm{d}t^2} + D\frac{\mathrm{d}x}{\mathrm{d}t} + Kx = f(x,i), \tag{10}$$

where $M$ is the total mass of the moving PM and piston; $D$ is the sum of the viscous damping of the clearance seal ($D_g$) and the equivalent damping of the compressing gas ($D_e$); $K$ is the sum of the flexure spring stiffness ($K_m$) and the equivalent stiffness of the gas spring ($K_g$). The gas spring effect on the piston can be expressed as the equivalent gas stiffness as follows:

$$K_g = \frac{(P - P_{mean})S_t}{x}. \tag{11}$$

The equivalent damping coefficient ($D_e$) of the compressed gas, reflecting the hysteresis loss caused by irreversible compression, as well as the viscous damping coefficient ($D_g$) can be obtained respectively in references [23,24].

### 3.2. Harmonic analysis

In order to obtain explicit solutions of Eqs. (9) and (10), the harmonic wave assumptions of input voltage, electrical current and displacement of the piston were used as

$$x(t) = x_a e^{j\omega t}, \tag{12}$$

$$i(t) = i_a e^{j(\omega t+\theta_1)}, \tag{13}$$

and

$$v(t) = v_a e^{j(\omega t+\theta_2)}. \tag{14}$$

Although there exist higher-order harmonic waves, the deformation of sine wave caused by them is actually small, and penalty of correction can be ignored [3,17]. As a result, the relation between the piston displacement and the current is

$$\frac{x_a}{i_a} = \frac{A_2}{\sqrt{(A_1 - M\omega^2)^2 + (D\omega)^2}}, \tag{15}$$

and the phase shift between the current and the displacement is

$$\theta_1 = \arctan\left(\frac{D\omega}{A_1 - M\omega^2}\right). \tag{16}$$

From Eqs. (15) and (16), it was found that when $A_1$ equals to $M\omega^2$ or in other words, when the resonant state of oscillation system is reached, the largest amplitude of the displacement can be obtained with a certain current input. In the same way, the relation between the piston displacement and the voltage is

$$\frac{x_a}{v_a} = \frac{1}{\sqrt{\left[\frac{R}{A_2}(A_1 - M\omega^2) - \frac{A_3}{A_2}D\omega^2\right]^2 + \left[\omega\left(R\frac{D}{A_2} + A_4 + \frac{A_3}{A_2}(A_1 - M\omega^2)\right)\right]^2}}, \tag{17}$$

and the phase shift between the applying voltage and displacement is

$$\theta_2 = \arctan\left(\frac{\omega\left(R\frac{D}{A_2} + A_4 + \frac{A_3}{A_2}(A_1 - M\omega^2)\right)}{\frac{R}{A_2}(A_1 - M\omega^2) - \frac{A_3}{A_2}D\omega^2}\right). \tag{18}$$

As a result, the phase shift between applied voltage and input current is

IPR2024-00569
Sony EX1018 Page 7

$$\theta = \theta_1 - \theta_2 = -\arctan\left(\frac{(A_3D^2\omega^3 + \omega A_2A_4(A_1 - M\omega^2) + \omega A_3(A_1 - M\omega^2)^2)}{R(A_1 - M\omega^2)^2 + \omega^2 D(RD + A_2A_4)}\right). \tag{19}$$

Substituting the expression of the electromagnetic force (Eq. (6)) into the following equation and integrating, the mechanical power of the linear motor is

$$p_m = \frac{1}{T}\int_0^T f(i,x)\,dx = \frac{\omega\mu_0\pi r}{l_1} H_o l_p N x_a i_a \sin\theta_1 = \frac{0.5Di_a^2}{\left(\frac{A_1 - M\omega^2}{A_2\omega}\right)^2 + \left(\frac{D}{A_2}\right)^2}. \tag{20}$$

The electrical input power of the linear motor is

$$p_{in} = \frac{1}{T}\int_0^T v\,di = \frac{1}{2} i_a v_a \cos\theta, \tag{21}$$

and the copper loss of the motor is

$$p_{Cu} = \int_0^T i^2 R\,dt = \frac{1}{2} i_a^2 R. \tag{22}$$

Finally, the motor efficiency defined as the ratio of the mechanical output from the motor to the electrical input power is

$$\eta = \frac{p_m}{p_{in}} = \frac{D}{R\left[\left(\frac{D}{A_2}\right)^2 + \left(\frac{A_1 - M\omega^2}{A_2\omega}\right)^2\right] + D}. \tag{23}$$

It can be seen that when the input power ($p_{in}$) is constant, the motor efficiency depends on two groups of design parameters. The first group is related to the operating conditions. The motor efficiency can be maximized when resonance is realized. The second group is determined by the motor size and material properties. The motor efficiency can be improved greatly when (1) the air gap become small, (2) both the magnet and coil sizes are large enough and (3) the coercive force of the PM becomes large.

### 3.3. Equivalent circuit of linear compressor

The compressor can be regarded as an inductance component which is important to the design of the drive and control circuit [24]. By combining Eq. (9) with Eq. (15), we have

$$\frac{v}{i} = (R + R_e) + j(L + L_e), \tag{24}$$

where

$$R_e = \frac{DA_2^2\omega^2}{(A_1 - M\omega^2)^2 + (D\omega)^2},$$

$$L_e = \frac{\omega(A_1 - M\omega^2)A_2^2}{(A_1 - M\omega^2)^2 + (D\omega)^2},$$

and

$$L = \omega A_3.$$

Here $R$ is the equivalent resistance of the copper loss and iron loss. $R_e$ is the equivalent resistance of the mechanical damping. $L$ is the inductance of the coil and $L_e$ is the equivalent inductance of the mechanical springs.

As a consequence, the moving magnet linear compressor can be expressed as an equivalent circuit, as shown in Fig. 9. According to the electric circuit theory, the inductive components absorb and discharge energy periodically, and the energy dissipation just happens on the resistance. Similarly, the mechanical power of the linear compressor can be regarded as the energy dissipation on the $R_e$, so it can be expressed as $0.5i_a^2R_e$. The motor efficiency can finally expressed by

$$\eta = \frac{R_e}{R + R_e}. \tag{25}$$

Substituting the expression of $R_e$ and $R$ into Eq. (25), the motor efficiency can be obtained which is identical to Eq. (23).

## 4. Experimental study of linear compressors

In order to investigate the dynamic performance of the linear compressor, a measurement system was built (see Fig. 10). The above-mentioned linear motor was used to provide driving force for compression. The moving magnet shuttle was supported on stainless steel suspension flexure springs, whose stiffness is shown in Table 1. A hollow piston was adopted to reduce the mass of the reciprocating assembly. In order to investigate the effect of piston mass on the natural frequency, two pistons with the identical dimensions were manufactured by aluminum (165 g) and stainless steel (483 g) respectively. The clearance seal between the piston and cylinder is 10–20 μm in width and 80 mm in length. The static leakage ratio to the swept volume is consequently less than 5%. A pure sine-wave power (TPS-500B) supplies single-phase alternating current to the primary coil of transformer (TDGC2M-5, 5 kW), the motor exciting coil has been connected with the secondary coil serially. As a result, large exciting current (maximum 15 A) can be provided to produce enough magnetic flux. The dynamic pressure signal was measured by the piezoelectric transducers (KISTEL 601A) and recorded by a digital oscilloscope. The displacement of the piston was measured by the strain signal of the flexure spring. Table 2 is the list of adjustable working conditions, by combination

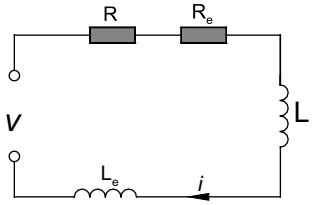



Fig. 9. Equivalent circuit of the linear compressor.

IPR2024-00569
Sony EX1018 Page 8

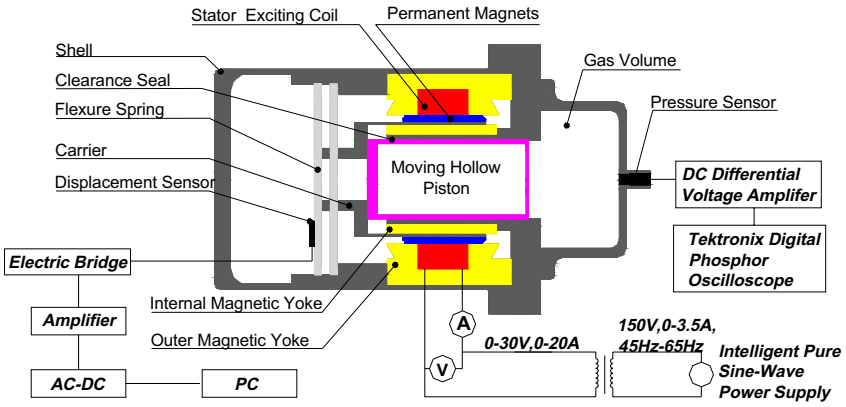



Fig. 10. Experimental apparatus of the moving magnet linear compressor.

Table 2
Working conditions of the linear compressor

| | | | | | | |
|---|---|---|---|---|---|---|
| Charging pressure (MPa) | 0.8 | 1.0 | 1.2 | 1.4 | 1.6 | 1.8 |
| Input voltage (V) | 5 | 10 | 15 | 20 | 24 | |
| Working frequency (Hz) | 45 | 50 | 55 | 60 | 65 | |

of which different experimental conditions had been realized.

Fig. 11 shows the influence of input voltage on the displacement of the piston under different operating frequencies. It is evident that the relationship between the input voltage and displacement is approximately linear and the increasing rates vary with the working frequency. At the working frequencies of 45 Hz and 65 Hz, the linear increasing rates are 0.47 mm/V and 0.12 mm/V, respectively. When the working frequency reaches its natural frequency, the increasing rate at this point is larger than that at other conditions.

The predicted strokes from Eq. (17) agree with the experimental results, especially at high working frequencies. The stiffness of the gas and damp coefficient play a key role on the accuracy of the prediction. In practice,

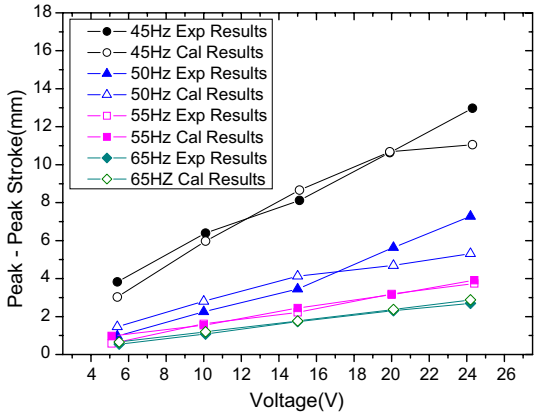



Fig. 11. Comparison of predicted voltage–stroke characteristics for different operating frequencies, with measured characteristic, at a charge pressure of 1.2 MPa.

the damp mainly involves the mechanical friction damping and the thermodynamic dissipation of the compression gas. Among them, the mechanical friction, depending on the magnitude of the clearance, can be measured in the process of assemblage by virtue of the vibrometer.

Fig. 12 shows the variations of the measured amplitude of the displacement, the pressure wave and the corresponding natural frequency under different working frequencies with the charging pressure ranging from 0.8 MPa to 1.8 MPa, at the constant input voltage of 20 V. The natural frequency can be obtained by $\omega_n = \sqrt{K/(M_{mover} + M_s/3)}$, in which the spring stiffness of gas ($K_g$) is from Eq. (11). It is clear that with the increase of charging pressure, natural frequency rises. When the working frequency is close to its natural frequency, larger stroke can be obtained. When the charging pressure is 1.4 MPa, the corresponding natural frequency is approximately 46 Hz, and the stroke at 65 Hz working frequency is smaller than that at 45 Hz.

The pressure wave actually does not reach its peak with the displacement wave synchronously. If the total mass of the gas in the compression chamber is assumed constant, the ideal gas law equation can be transformed to $\Delta P/\Delta V = P_{mean}/V_{mean}$, in which $\Delta V$ equals to $S_t \Delta x$. It can be found that the amplitude of the pressure wave is related to the charging pressure and the variation of the piston stroke.

Finally, the natural frequency is not a simple function of charging pressure and is also influenced by the stroke [25]. When the working frequencies ranges from 45 Hz to 55 Hz, the influence of them on the natural frequency is less than 10% with the charging pressure ranging from 0.8 MPa to 1.8 MPa (see Fig. 12). However, when the working frequency is 65 Hz, the corresponding natural frequency (40 Hz) is very low due to the weak stiffness of the compressed gas.

The frequency responses of two different pistons are shown in Fig. 13. The mass of the two shuttles are 767 g and 1085 g respectively. As for the aluminum piston, at the charging pressure of 1.6 MPa and the applied current of 10 A, the measured pressure amplitude is 365 kPa, the peak–peak stroke is 11.34 mm and the natural frequency

IPR2024-00569
Sony EX1018 Page 9

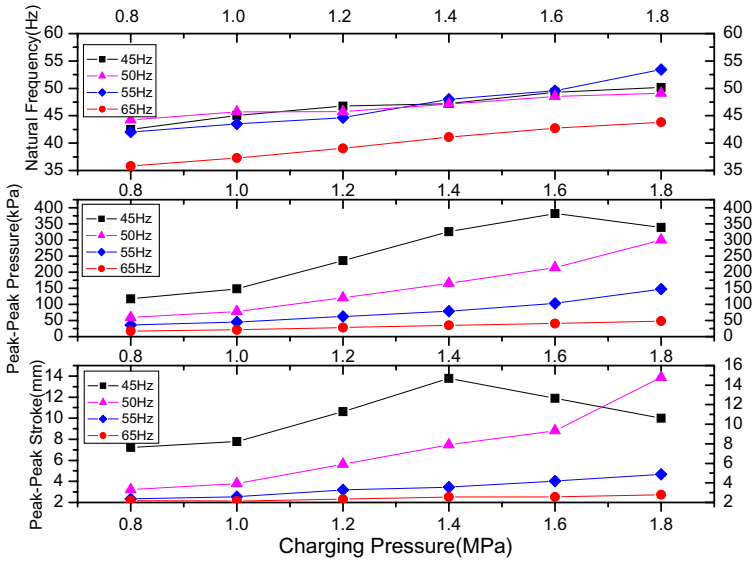



Fig. 12. Measured displacement, pressure wave and natural frequency vs. charging pressures for different operating frequencies at 20 V input voltage.

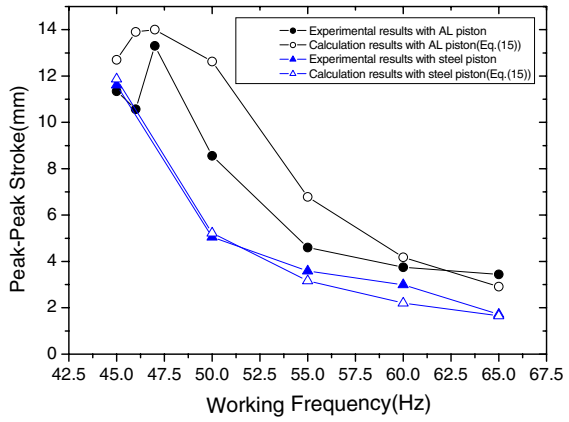



Fig. 13. Comparison of predicted frequency–stroke characteristics for different shuttles, with measured characteristics, at a charge pressure of 1.6 MPa and 10 A input current.

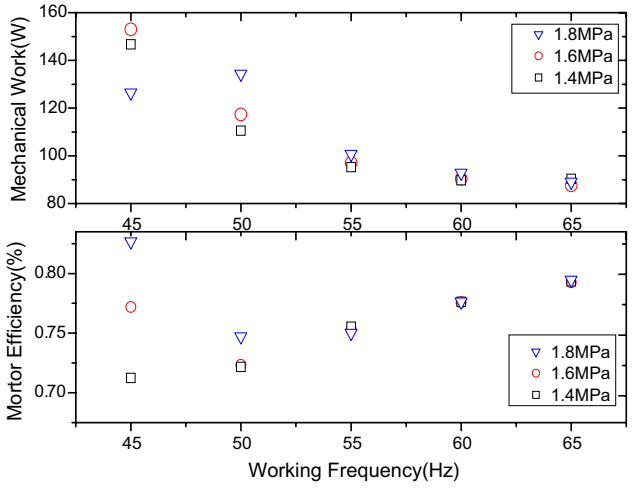



Fig. 14. Measured motor efficiency and mechanical work vs. working frequency at the input voltage of 15 V and different charging pressures.

is 48 Hz. When the exciting current is constant, there exists a peak of stroke when the working frequency is close to its natural frequency. Comparatively, the natural frequency of the steel piston is about 40 Hz at 1.6 MPa charging pressure and 10 A input current. In consequence, the stroke decreases with the increase of the working frequency. Therefore, the reasonable configurations and materials should be adopted to ensure good system performance.

Neglecting the influence of other parameters in Eqs. (20) and (23), both efficiency and mechanical work of the compressor are decided by the term of $(A_1 - M\omega^2)/A_2\omega$. It can be found that when $A_1 \geqslant M\omega^2$, this term will decrease with the increase of working frequency; when $A_1 < M\omega^2$, the value of this term will increase with the increase of working frequency. In Fig. 14, when the working frequency approaches to its natural frequency, the mechanical work is always higher. However, the point of maximum efficiency is not the point of maximum work. For instance, at the charging pressure of 1.8 MPa, the natural frequency is about 50 Hz. The peak of efficiency 83% happens at the working frequency of 45 Hz, contrastively the maximum work output of 134 W happens at the resonant point. According to Fig. 14, it can be found that the efficiency decreases and the output work reaches its peak at the resonant point. When the resonant happens, the stroke is correspondingly maximized, and the damping reaches its peak. Hence, the efficiency may decrease a little, according to Eq. (23). In the experimental study, it can be observed that when the resonance happens, the current was always be maximized with the same input voltage and the mechanical work was also be maximized. In addition, the maximum current as well as the stroke will produce large energy dissipation. That is the reason why the maximum efficiency cannot obtained at the resonant state. Generally, the working frequency should be regulated a bit lower than its

IPR2024-00569
Sony EX1018 Page 10

natural frequency. Only at this condition, the relative high efficiency and large output work can be obtained simultaneously.

## 5. Conclusions

The static force characteristics of the moving magnet linear motor have been studied by the magnetic circuit analysis and numerical FEA, and verified by experimental investigations. The expression of the force against the displacement of the piston was deduced, which can actually be divided into three parts, one is the force caused by the exciting current; the other two terms whose magnitude has close relationship with the displacement of the piston, are the force interacting between the PM and the ferrite yoke. Based on these expressions, the optimization operating point of the PM was analyzed. The static equilibrium characteristics of the PM, including two steady equilibrium and one unsteady equilibrium points, and its effects were also revealed.

In order to investigate the performance of the linear compressor, a mathematical model has been developed, which includes the model of the linear motor, thermodynamics of compressing gas and driving electric circuit. Based on the harmonic solutions of the mathematical model, an equivalent circuit of the linear compressor was deduced. A set of expressions concerning the mutual relations between the voltage, current, stroke, phase shift, mechanical work and motor efficiency were obtained. In addition, a prototype of the linear compressor was developed and corresponding experimental analysis were conducted. Both the experimental and theoretical results indicate that the motion of the moving piston complies with the principle of oscillation dynamics. The stroke is approximately a linear function with the input voltage. The optimal working frequency should be a bit lower than its natural frequency.

## Acknowledgements

The work has been supported by the National Natural Science Foundation of China under the contract No. 50376069. The manufacture of the linear compressor and the corresponding experimental studies were carried out at Shanghai Institute of Technical Physics.

## References

[1] Redlich R, Unger R, Van der Walt NR. Linear compressor: motor configuration, modulation and systems. In: Proceeding of the international compressor engineering conference, July 1996. p. 23–6.

[2] Clark RE, Smith DS, Mellor PH, Howe D. Design optimization of moving magnet actuators for reciprocating electro-mechanical systems. IEEE Trans Magnet 1995;31(6):3746–8.

[3] Shirey K, Banks S. Design and qualification of the AMS-02 flight cryocoolers. Cryogenics 2006;46:143–8.

[4] Nast T, Olson J, Champagne P, et al. Overview of Lockheed Martin cryocoolers. Cryocooler 2006;46:164–8.

[5] Longthworth RC. Three-stage linear, split-Stirling cryocooler for 1 to 2 K magnetic cold stage. NASA Contract Report 4538, 1993.

[6] Byckling E, Perkio K. Dynamic properties of moving magnet transducers. IEEE Transactions on magnetics 1980;16(2):468–73.

[7] Yang CH, Nasar SA, Yount WR. Novel high force–density PM linear oscillating motors and their controllers. In: Proceedings of the applied power electronics conference and exposition, March 1989. p. 183–7.

[8] Poornima KA, Hsu TS. Moving magnet loudspeaker system with electronic compensation. IEE Proc Circ Dev Syst 2001;148(4):211–5.

[9] Ebihara D, Watada M. Development of a single-winding linear oscillatory actuator. IEEE Trans Magn 1992;28(5):3030–2.

[10] Clark RE, Jewell GW, Howe D. Dynamic modeling of tubular moving-magnet linear actuators. J Appl Phys 2003;93(10):8787–9.

[11] Clark RE, Jewell GW, Howe D. Finite element analysis of short-stroke linear motors and actuators. IEE Colloquium (Digest) 2000;13(Jan):41–6.

[12] Liu J, Steven G. Characterization of a small moving magnet electrodynamic linear motor. J Acoust Soc Am 2005;118(4):2289–94.

[13] Cadman RV, Cohen R. Electrodynamic oscillating compressors: Part 1 – Design based on linearized loads. Trans ASME J Basic Eng 1969;12:657–63.

[14] De Jonge AK. Analysis and optimization of a linear motor for the compressor of cryogenic refrigeration. Adv Cryogen Eng 1981;27:631–40.

[15] Pollak E, Soedel W, Cohen R. On the resonance and operational behavior of an oscillating electrodynamics compressor. J Sound Vib 1979;67(1):121–33.

[16] Cadman RV, Cohen R. Electrodynamic oscillating compressors: Part 2 – Evaluation of specific designs for gas loads. Trans ASME J Basic Eng 1969(December):665–70.

[17] Koh DY, Hong YJ, Park SJ, Kim HB, Lee KS. A study on the linear compressor characteristics of the Stirling cryocooler. Cryogenics 2002;42(6):427–32.

[18] Unger R. Development and testing of a linear compressor sized for the European market. www.sunpower.com/lib/sitefiles/pdf/publications/doc0074.pdf.

[19] Van der Walt NR. Linear compressors – a maturing technology, www.sunpower.com/lib/sitefiles/pdf/publications.doc0054.pdf.

[20] Van der Walt NR, Unger, R. The simulation and design of a high efficiency lubricant free, linear compressor for domestic refrigeration. In: Proceedings of the international compressor engineering conference, July 1992. p. 14–7.

[21] Keung C, Patt PJ, Starr M, et al. Design and fabrication of a long-life Stirling cycle cooler for space application, phase III – prototype model. Final Report, September 1981–September 1990, Philips Laboratories.

[22] Fitagerald AE, Charles K, Stephen DU. Electric machinery. 6th ed. New York: McGraw-Hill; 2003.

[23] Israel Urieli, Berchowitz DM. Stirling cycle engine analysis. Bristol: Adam Hilger; 1984.

[24] Yu YZ, Liu Y. Special compressor. Beijing: China Machine Press; 1998.

[25] Park SJ, Hong YJ, Kim HB, et al. The effect of operating parameters in the Stirling cryocooler. Cryogenics 2002;42:419–25.

IPR2024-00569
Sony EX1018 Page 11